Science of the Total Environment 732 (2020) 139281

Contents lists available at ScienceDirect

Science of the Total Environment

journal homepage: www.elsevier.com/locate/scitotenv

COVID-19 pandemic persuaded lockdown effects on environment over stone quarrying and crushing areas

Indrajit Mandal [1,*], Swades Pal [1]

Department of Geography, University of Gour Banga, Malda, India

HIGHLIGHTS

- Particulate matter concentration by three to four times amid lockdown.
- Surface temperature is reduced by 3–5 °C.
- Amid lockdown noise level is reduced from 85dBA to <65dBA.
- Total dissolve solid concentration in river water is reduced by two times.

GRAPHICAL ABSTRACT

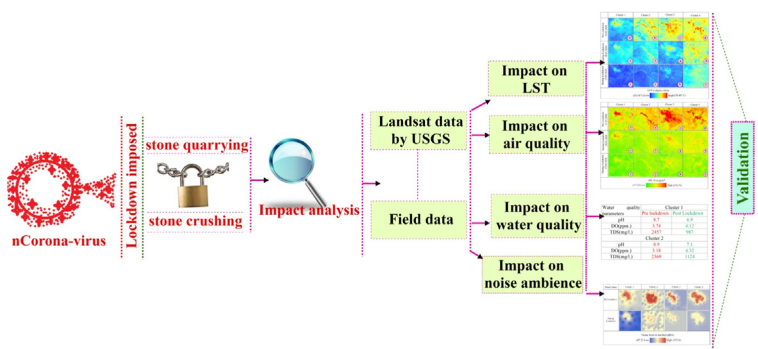

ARTICLE INFO

Article history:
Received 26 April 2020
Received in revised form 30 April 2020
Accepted 6 May 2020
Available online 11 May 2020

Keywords:
Lockdown
Environmental components
Concentration of particulate matter
Noise pollution
Surface temperature
River water quality

ABSTRACT

Stone quarrying and crushing spits huge stone dust to the environment and causes threats to ecosystem components as well as human health. Imposing emergency lockdown to stop infection of COVID 19 virus on 24.03.2020 in India has created economic crisis but it has facilitated environment to restore its quality. Global scale study has already proved the qualitative improvement of air quality but its possible impact at regional level is not investigated yet. Middle catchment of Dwarka river basin of Eastern India is well known for stone quarrying and crushing and therefore the region is highly polluted. The present study has attempted to explore the impact of forced lockdown on environmental components like Particulate matter (PM) 10, Land surface temperature (LST), river water quality, noise using image and field derived data in pre and during lockdown periods. Result clearly exhibits that Maximum PM_{10} concentration was 189 to 278 μg/m^3 in pre lockdown period and it now ranges from 50 to 60 μg/m^3 after 18 days of the commencement of lockdown in selected four stone crushing clusters. LST is reduced by 3–5 °C, noise level is dropped to <65dBA which was above 85dBA in stone crusher dominated areas in pre lockdown period. Adjacent river water is qualitatively improved due to stoppage of dust release to the river. For instance, total dissolve solid (TDS) level in river water adjacent to crushing unit is attenuated by almost two times. When entire world is worried about the appropriate policies for abating environmental pollution, this emergency lockdown shows an absolute way i.e. pollution source management may restore environment and ecosystem with very rapid rate.

* Corresponding author.
E-mail address: indrajitgeofarakka@gmail.com (I. Mandal).
[1] Both authors equally contributed.

https://doi.org/10.1016/j.scitotenv.2020.139281
0048-9697/

1. Introduction

Outbreak of COVID 19 and worldwide lockdown situation has immense negative impact on world's economy but environment has got rid off from the huge anthropogenic pressure like huge emission of pollutants of different kinds (Ray et al., 2020; Beine et al., 2020; Huang et al., 2020; He et al., 2020; Wu et al., 2020; Mahato et al., 2020). This lockdown situation has created a golden opportunity to judge the anthropogenic intervention on qualitative degradation of environmental components at very local to global scales (Anjum, 2020; Becchetti, 2020; Cadotte, 2020; Das et al., 2020; Layard et al., 2020; Saadat et al., 2020). COVID-19 outbreak was first reported from Wuhan, China on 31st December 2019. With >1 million novel coronavirus infections and about 50,000 deaths in the world at the end of March 2020 and almost 200,000 deaths as on 26.04.2020, the researchers are looking into the existence of the virus and assessing its short and long term effects (Isaifan, 2020; Dutheil et al., 2020; Han et al., 2020). The mortalities of this infection were not above 3.4% worldwide, given its adverse effects which compel the World Health Organization to declare COVID-19 as a public health emergency of international concern. To cope with COVID-19 pandemic, it has become clear to the world, the Chinese model of social distancing is mandatory without any alternative (Huang et al., 2020; Zhang et al., 2020). The WHO announced on 30th January 2020 that COVID-19 was Chinese epidemic to be an international public health emergency posing a high risk to vulnerable health care system (Sohrabi et al., 2020; Kambalagere, 2020). Most of the countries of the world have adopted the way of lockdown over the advance of time to combat with this fatal virus in spite of having possibility of landslide in economy.

Due to complete halt of industrial, transport, tourism sectors, the adverse effects of these economic activities on environment has reduced considerably. Crude fact is that deaths from air pollution accounted for 7.6% of all fatalities worldwide as per 2016 report by WHO (WHO, 2020; Isaifan, 2020). So, such reduced pollution level could be help nature to restore herself and help people to get fresh breath (Kelly and Fussell, 2015; Wu et al., 2017; Ma et al., 2020; Yongjian et al., 2020; Sharma et al., 2020; Raffaelli et al., 2020). In China, NO_2 and carbon emissions have reduced respectively by 30 and 25% (Lauri, 2020; McMahon, 2020). Watts and Kommenda (2020) have also shown same kind of effect due to industrial shutdown and temporary cuts in air emissions worldwide (Chowdhury et al., 2019; Mathur et al., 2020). As per McMahon (2020), the lockdown has reduced the level of pollution in China that has led to the lives of 77,000 people indirectly. The European Space Agency (2020) reported, between 1st January 2020 and 11 March 2020, a significant decrease in nitrous oxide emissions from the Po valley region in Northern Italy in vehicles, power plants and farms, with national lockdowns. The average Particulate Matter (PM) 2.5 level in the Indian capital, New Delhi, was reduced by 71% over the past weeks from 91 μg/m^3 on March 20 to 26 μg/m^3 on March 27, after the lockdown began. (CPCB, 2020; Mate et al., 2020; Mitra et al., 2020). Over the same time, Nitrogen Dioxide was reduced from 52 to 15 μg/m^3 (about 71%). There has also been a decrease in such air contaminants in Mumbai, Chennai, Kolkata and Bangalore (CPCB, 2020; Sharma et al., 2020 Lau et al., 2020). CPCB's (2020) analysis also found that the national Janta Curfew in India on 22 March resulted in record lowest rate of 1 day traffic emissions (CPCB, 2009). $PM_{2.5}$ and Pm_{10} were also steeply decreasing. Between 23 and 29 March, the most prominent NO_2 decrease was observed when the concentration dropped to 10 μg/m^3. He et al. (2020) reported that the Air Quality Index and $PM_{2.5}$ concentrations is decreased by 25% during the lock-off time spanning a few weeks while worked with Chinese cities. Cadotte (2020) also reported decreasing air pollutants over major cities of the world where the outbreak is very strong. In Seoul, capital of South Korea, $PM_{2.5}$ has reduced by 54% in lockdown period than the same time of the previous year. In Wuhan, air quality is improved by 44%. Ogen (2020) has found a strong link between the concentration of NO_2 and fatality caused by COVID-19 in another study of areas in Italy, Spain, France, and Germany. Lee et al. (2011), Yap et al. (2011), Yap and Hashim (2013), Chitranshi et al. (2015); Pal and Mandal (2019a, b), Chowdhury et al. (2019), Olmanson et al. (2016), Alvarez-Mendoza et al. (2019) have warned about the growth of PM concentration in lower atmosphere due to human activities. Most of them had computed the PM using either Landsat or MODIS products. Concentration of greenhouse gases like SO_2, NO_2, CO, PM etc. are considered as dominant causes of temperature rise in atmosphere. Bashir et al. (2020) found a linkage between air quality parameters and climate parameters like temperature, humidity, air movement etc. Andersson and Nässén (2016), Jerez et al. (2018), Manabe (2019) reported that the high accumulation of greenhouse gases may augment the temperature and associated other climatic components like fog, dew, precipitation etc. Along with such global level studies a few works have also done in Indian subcontinent. Sharma et al. (2020) reported concentration of $PM_{2.5}$, PM_{10}, CO_2, NO_2, ozone (O_3) and SO_2 over 22 cities of India in March and April 2020 and compared the result with same window time of 2017 in order to explain air quality improvement in India. This lockdown is a breakthrough in this mounting concern. Along with air quality, noise pollution is reduced as transport and industry are the major sources of noise (Tonne et al., 2016; Wang et al., 2020; Abdullah et al., 2020). It is to be mentioned that due to noise pollution so many people experiences direct and indirect harms over the world (Pal and Mandal, 2019a, b). Deafness, high blood pressure, heart failure are some of the crudest consequences of noise. Worldwide, 360 million peoples are prone to hearing loss due to noise. Out of them, 27% and 22% are in South and East Asia respectively. Among different forms of noises, noise at occupational place is the most crucial reason behind hearing loss (WHO, 2012).Significant reduction of pollutant water from the different economic sectors is noticed. The New Indian Express on 24.04.2020 reported that water quality of river Ganga, in India is improved by 40–50% during the time of lockdown. CPCB (2020) reported that Dissolved oxygen (DO) (>6 mg/l), Biochemical oxygen demand (BOD) (<2 mg/l), total coliform (5000 per 100 ml) and pH (range between 6.5 and 8.5) have improved a lot and the identified range of the quality components are within the range of bathing. Different Government reports, reports of the researchers have heighted the glimpse of the effects of COVID 19 pandemic over the major cities of the world. The present work intends to focus on the effects of COVID 19 on the environmental components of stone mine and crushing industries dominated middle catchment of Dwarka river basin.

The Dwarka River - a tributary of Mayurakshi is a well-known name in the river scenario of West Bengal and Jharkhand states of Eastern India. The middle catchment of the basin (area: 3883 km^2) is rich with crystalline granite rocks as these are the extended parts of Chottanagpur plateau. There are 239 stone mining and 982 stone crushing centres at the very vicinity of residential areas of poor economic background (Fig. 1). These mining & crushing centres are used to produce approximately ~258,120 tons of dust per year (Pal and Mandal, 2017) and it causes serious threats to the environmental components like air, water, soil (Pal and Mandal, 2017; Pal and Mandal, 2019a; Pal and Mandal, 2019b). These stone quarrying and crushing centres are in operational mode almost every day of the year. But when the Indian government announced the country lockdown on 24.03.2020 to prevent the infection of the COVID-19, these were shut down temporarily. For in-depth spatial analysis, we have selected four densely found quarrying and crushing areas from the middle catchment defining cluster 1 to 4 with an area of 19.36 km^2 each. Entire river basin possesses more than ten such mining and quarrying clusters but purposively we have selected those four where the frequency of crushing unit is maximum. These quarrying and crushing units have generated livelihood opportunity but huge dust emission in different forms have negative impact on environment and human health (Pal and Mandal, 2019a, b; Han et al., 2020). Policy makers are worried for formulating suitable abatement policies. Researchers at global level have reported the positive impact of lockdown on air quality. But its possible impact at regional and

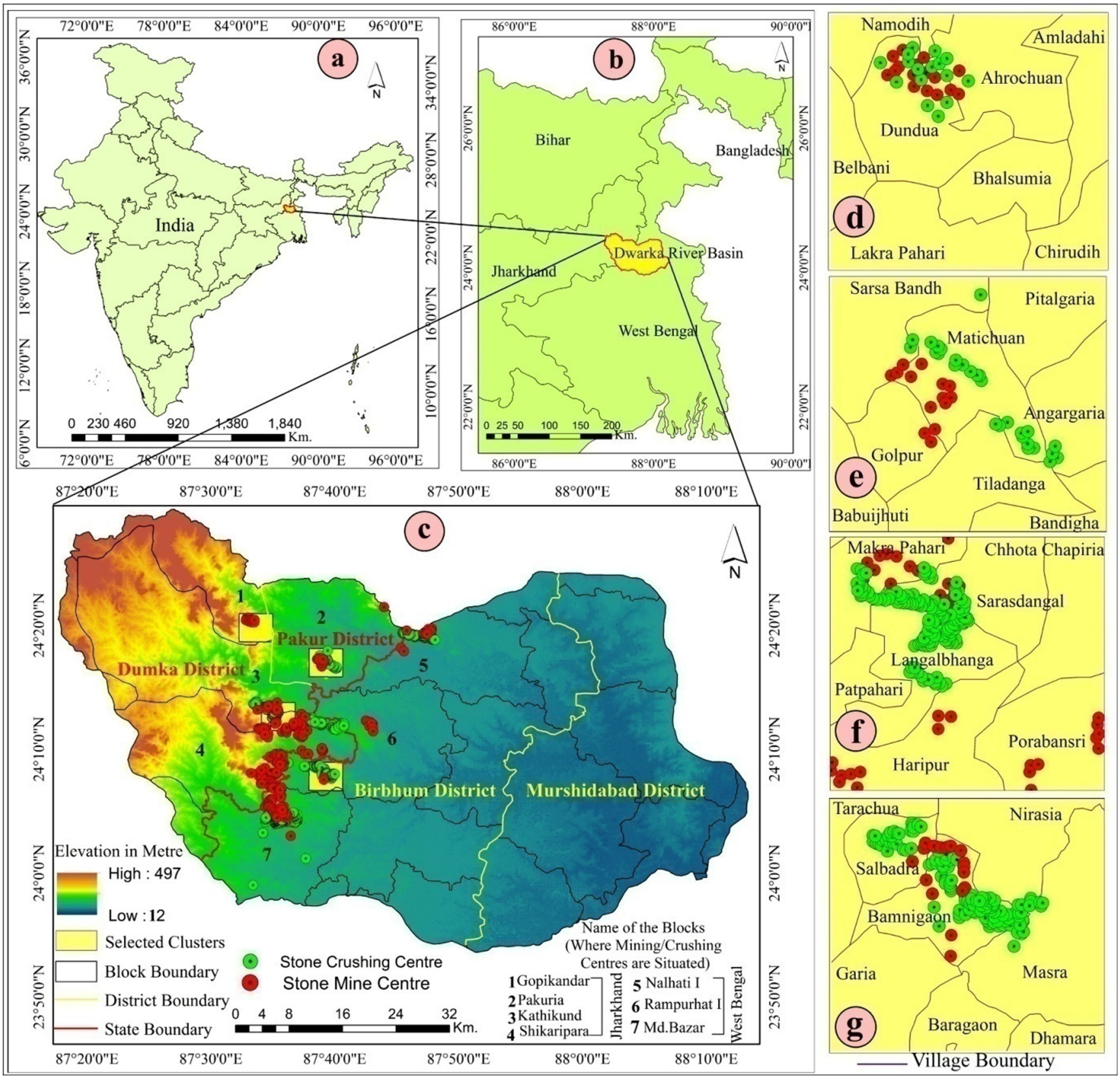

Fig. 1. Location of the study area: (a) Dwarka river basin within India and (b) Geographical extension of the basin within Jharkhand & West Bengal (c) selected clusters within the Dwarka river basin (d–g) Clusters 1 to 4 with village boundary.

local scale is yet not explored. Considering this gap of research the present study has intended to explore the impact of lockdown on environment in general and some specific environmental components like on PM concentration in air, change of land surface temperature, noise ambience and river water in the stone quarrying and crushing dominated areas of Eastern India.

2. Materials

Landsat 8 OLI image (path 139 and row 43 and spatial resolution 30 m) of the United States Geological Survey (USGS) has been used for LST and PM_{10} mapping. PM_{10}, LST has been extracted from the downloaded satellite images for the dates of 12-March-2020 as a representative of pre lockdown time and 28-March-2020 and 13-April-2020 as the representative of ongoing lockdown periods. Noise level is recorded from field. Water samples from river have also taken from the field from 12 sites. Water quality data of the pre lockdown time is taken from Pal and Mandal (2019a).

3. Methods

3.1. Computation of aerosol from Landsat image and validation

Radiometric correction has been applied to transform the DN values into radiance or the reflectance values. This is then converted at sensor radiation into radiances on the surface of the earth following Chander et al. (2009), (Eq. (1)).

$$L\lambda = ML * Qcal + AL \tag{1}$$

The Landsat 8 OLI band data will then be converted into TOA spectral radiance using the rescaling factors in order to extract the Top of Atmospheric Radiance (TAR). The rescaling factors are given in the image metadata file.

$$L\lambda = ML * Qcal + AL \tag{2}$$

where, Lλ = Top of atmospheric radiance, ML and AL = Multiplicative and additive rescaling factor of the particular band, Qcal = Quantized pixel value.

Then we need to DN value to Conversion of digital number to Top of Atmospheric reflectance. We need the reflectance rescaling coefficient for conversion. The metadata file contains the reflectance rescaling coefficient. For the conversion the following equation was used (Eq. (3)).

$$\rho\lambda' = M\rho * Qcal + A\rho \tag{3}$$

where, ρλ′ = top of atmospheric (TOA) planetary reflectance. But here it should be noted that planetary reflection at the top of the atmosphere does not involve sun angle correction. Mρ = multiplicative rescaling factor, Aρ = additive rescaling factor, Qcal = quantized calibrated pixel.

The sun angle of the top reflection of the atmosphere was determined using the following formula for correction (Eq. (4))

$$\rho\lambda' = \frac{\rho\lambda'}{\cos(\theta SZ)} = \frac{\rho\lambda'}{\sin(\theta SE)} \tag{4}$$

where, ρλ = Top of Atmospheric (TOA) planetary reflectance, θ_{SE} = Local sun elevation angle, θ_{SZ} = local solar zenith angle. For the measurement of the solar zenith angle we used the solar elevation (provided in metadata). (Eq. 5)

$$\theta_{SZ} = 90\,^{\circ} - \theta SE \tag{5}$$

The goal of air correction is to eliminate the various atmospheric effects that affect the signal the sensors receive. For multi-spectral satellite imaging, there are so many approaches and techniques. The following equation has been used here in the measurement of reflection on the land surface (Eq. 6).

$$\rho = \frac{\pi * (L\lambda - Lp) * d^2}{Tv * \{(ESUN\lambda * \cos\theta SZ * TZ) + Edown\}} \tag{6}$$

where, ρ = land surface reflectance, L_P = path radiance, T_V = atmospheric transmittance in the viewing direction, T_Z = the atmospheric transmittance in the illumination direction, Edown = the down welling diffuse irradiance, ESUNλ = solar *exo*-atmospheric irradiances, d = earth sun distance.

The elimination of path radiance is one of the main atmospheric corrections required to extract respiratory particulates from Landsat 8 image. Dark object subtraction method is currently the frequently used method for calculating the Landsat 8 data's path radiance. The Dark Object Subtraction's prime principle is in determining the dark object. So the path radiance was extracted using the equation below (Sobrino et al., 2004) (Eq. (7)).

$$L\rho = L\ \min - 0.01 * \frac{ESUN\lambda * \cos(\theta sz)}{\pi * d^2} \tag{7}$$

After processing the radiometric & atmospheric correction the atmospheric reflectance has been calculating by the subtracting the top of atmospheric (TOA) reflectance and the reflectance of the surface. On the basis of the aforementioned principle the aerosol optical thickness (AOT) has been calculated using the following equation.

$$AOT(\lambda) = aoR(\lambda) \tag{8}$$

$$R(\lambda) = \rho a(\theta sz, \theta v, \phi) \tag{9}$$

$$ao = \left(\frac{4\mu\mu o}{\omega o Pa(\theta sz, \theta v, \phi)}\right) \tag{10}$$

where, R (λ) = atmospheric reflectance comparable to wavelength region (λ) for satellite, Pa (θ_{SZ}, θ_v, φ) = the function of the aerosol scattering phase, θ_{SZ} = solar zenith angle (local), θ_v = viewing zenith angle, φ = the relative azimuth angle, μ = icosines of the view directions, μo = cosines of the illumination directions and ωo = albedo sing-scattering.

This equation can also be written as following for the three bands

$$AOT = aoR\lambda 1 + a1R\lambda 2 + a2R\lambda 3 \tag{11}$$

where, $R\lambda_{1/2/3}$ = atmospheric reflectance (1, 2 and 3 comparable to wavelength region for satellite), a = the algorithm coefficient.

The aerosol optical thickness and particulate matter relationship is defined as a single homogeneous atmospheric layer comprising the spherical aerosol particles. Koelemeijer et al. (2006) stated in his paper that the concentration of aerosol mass at the lower atmosphere of the earth's surface is obtained by drying sampled air.

$$PMX = \frac{4}{3}\pi\rho \int_0^{x/2} r^3 n(r) dr \tag{12}$$

The particulate matter (PM) is therefore predicted to be highly correlated with the optical aerosol (AOT) thickness. The method for estimating particulate matter concentrations is developed by Nadzri et al. (2010) using the spectral aerosol optic thickness (AOT) recovery.

$$PM_{10} = aoR\lambda 1 + ajR\lambda 2 + a2R\lambda 3 \tag{13}$$

where, $R\lambda 1_{/2/3}$ = atmospheric reflectance ($R\lambda_{1/2/3}$ is the corresponding to wavelength for satellite), $A_{0/1/2}$ = the algorithm coefficient which are empirically determined.

The particulate matter 10 (PM_{10}) is related to the atmospheric relectance and it is computed by the use of proposed algorithm (Nadzri et al., 2010) on the basis of highest R & lowest root mean square error (RMSE) values. In this case the highest correlation coefficient value is 0.888.

$$PM_{10} = 396R\lambda 2 + 253R\lambda 3 - 194R\lambda 4 \tag{14}$$

After computing and mapping PM_{10}, validation of the map is done using Tem-top airing-1000 air quality monitor (measuring range 0–999 μg/m^3, resolution 0.1 μg/m^3) derived field data at 80 sites on the same dates of image acquisition. Pearson's correlation coefficient is computed between the data derived from PM_{10} image and field data.

3.2. Method for extracting LST

Every object emits the thermal electromagnetic energy when its temperature is above the absolute zero (K). Considering this fact LST of different objects is calculated. The thermal sensor (TM/ETM/TIRS) received the signals and this signal can be converted to the at sensor radiance. There are so many methods are available for extracting the LST. Among different methods of extracting LST from the Landsat image,

Table 1
Water quality of the different parameters according to the BIS standards IS 10500 (2012).

Parameters	For drinking	For outdoor bathing	For irrigation
PH	6.5–8.5	6.5–8.5	6–8.5
DO (ppm.)	5	5	–
TDS(mg/l.)	500	–	2250

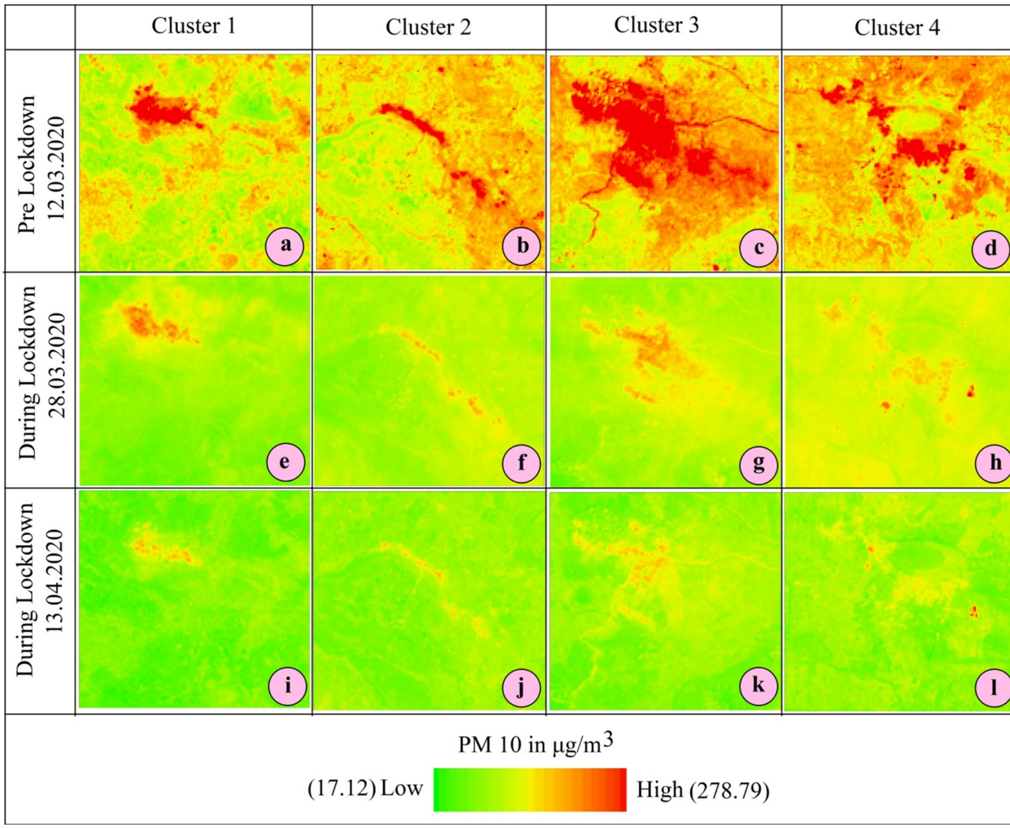

Fig. 2. Cluster wise particulate matter 10 in pre lockdown and during the lockdown period.

the method devised by the Landsat Project Science Office (LPSO) (2002) is as applied.

3.2.1. Pixel value or DN value conversion to spectral radiance (Lλ)

The spectral radiance (Aλ) is calculated using Eq. (15) given by Landsat Project Science Office (2002).

$$L\lambda = \text{“}gain\text{”} + DN + \text{“}bias\text{”} \tag{15}$$

where, L_λ = the spectral radiance of the specific thermal band, "gain" = digital number (DN) conversion function, DN = pixel value or digital number of a given pixel, "*bias*" = bias is the intercept of the Digital Number conversion function.

Eq. (15) can also be expressed as following:

$$L\lambda = \left(\frac{LMAX\lambda - LMIN\lambda}{QCALMAX - QCALMIN}\right) * (QCAL - QCALMIN) + LMIN\lambda \tag{16}$$

where, $QCAL_{min} = 0$, $QCAL_{max} = 255$, QCAL = quantized calibrated pixel value or digital number of each pixel, $LMIN_\lambda$ = spectral radiance for the thermal band at digital number 0 LMAX λ = spectral radiance for the thermal band at digital number 255.

3.2.2. Estimation of at satellite brightness temperatures (TB) from spectral radiance (Lλ)

For extracting the Land Surface Temperature the spectral radiance of the thermal bands of TM/ETM/TIRS are need to converted to the at-satellite brightness temp (TB). For this conversion we use Eq. (17) of LPSO (2002) formula.

$$TB = \frac{Kj}{\ln\left(\frac{Ki}{L\lambda} + 1\right)} \tag{17}$$

where, TB refers to at-satellite brightness temperature (K), $L\lambda$ spectral radiance of the thermal band in $W{\cdot}m^{-2}{\cdot}sr^{-1}.\ \mu m^{-1}$, K_i and $K_j = K_i$ and K_j both are the Calibration constant. (The calibration constants are provided in the metadata file of the particular image).

3.2.3. Land surface temperature (LST) and validation

The above obtained thermal value is referred to a black body. So the corrections for spectral emissivity are required and this correction can be done as per the nature of the land cover of that specific area (Snyder et al., 1998).The another way is also availabe in this case.

Table 2
Cluster wise levels of PM_{10} (μg/m^3) in pre lockdown and during the lockdown periods.

Phase	Cluster 1			Cluster 2			Cluster 3			Cluster 4		
	Max.	Avg.	Min	Max.	Avg.	Min	Max.	Avg.	Min	Max.	Avg.	Min
12.03.2020	189.45	139.44	67.55	248.49	189.69	69.88	278.79	259.25	82.45	227.58	201.55	79.68
28.03.2020	59.67	85.23	23.13	53.68	51.22	24.32	64.88	61.79	26.36	64.88	61.59	37.48
13.04.2020	49.55	47.22	22.35	44.87	42.55	23.24	49.46	47.47	23.36	49.54	47.78	25.26

Table 3
Clusterwise area under different PM_{10} levels.

PM_{10} classes ($\mu g/m^3$)	Area in cluster 1 (km^2)	Area in cluster 2 (km^2)	Area in cluster 3 (km^2)	Area in cluster 4 (km^2)
12.03.2020_Pre lockdown				
<50	4.78	3.66	1.24	1.67
50–100	4.75	3.98	1.89	1.88
100–150	6.64	8.74	4.36	9.32
>150	3.19	2.98	11.87	6.49
28.03.2020_During lockdown				
<50	16.88	18.11	12.14	9.89
50–100	2.47	1.25	7.22	9.47
100–150	Nil	Nil	Nil	Nil
150–200	Nil	Nil	Nil	Nil
13.04.2020_During lockdown				
<50	19.36	19.36	19.36	19.36
50–100	Nil	Nil	Nil	Nil
100–150	Nil	Nil	Nil	Nil
150–200	Nil	Nil	Nil	Nil

From the Proportion of vegetation values the emissivity of each pixel has been derived.

$$\textit{Land surface emissivity}(\varepsilon) = 0.004 * Pv + 0.986 \tag{18}$$

where, Pv = proportion of vegetation, Pv or proportion of vegetation is calculated using the following formula.

$$P_v = \frac{NDVI_{Jr} - NDVI_{\min}}{NDVI_{Jr} - NDVI_{\min}} \tag{19}$$

The emissivity corrected LST were computed using the following equation (Artis & Carnahan, 1982).

$$LST = TB/[1 + \{(\lambda * TB/\rho) * ln\varepsilon\}] \tag{20}$$

where, LST = land surface temperature in Kelvin, λ = wavelength of emitted radiance in metres, TB = at sensor brightness temperature (K), $\rho = h^*c/\sigma$ (1.438×10^{-2} m K), σ = Boltzmann constant (6.626×10^{-34} J s), c = velocity of light ($2.998 * 10^8$m/s) ε = emissivity (ranges between 0.97 and 0.99).

For validating the LST maps, LST is recorded from field on 80 sites using Digital Infrared Thermometer (Type-K) and Pearson correlation coefficient is computed between image and field based LST data.

3.3. Noise measurement

Stone crusher units emit heavy noise. Noise intensity is recorded using sound meter (digital noise level analyzer (type LT SL 4010) at 245 sites in pre lockdown phase and 37 sites from the same amid lockdown. Sites were selected not only at very proximity of crusher unit but also apart from the units. Field data at more sites have not been done during lockdown. Based on the recorded noise isopleth maps of four cluster have been generated for both the periods.

3.4. Measuring water quality

Total 12 water samples have been collected from adjacent rivers of four cluster and tested the pH, total dissolved solid (TDS), dissolved oxygen (DO). Water quality report of those sites for pre lockdown period has been collected from published article of Pal and Mandal (2019a). Average water quality is taken as comparison. Table 1 depicts the reference ambient water quality limits.

4. Results

4.1. Changing scenario of particulate matter 10 (PM_{10})

Fig. 2 shows the PM_{10} before the lockdown and during the period of lockdown in selected four densely concentrated quarrying and crushing

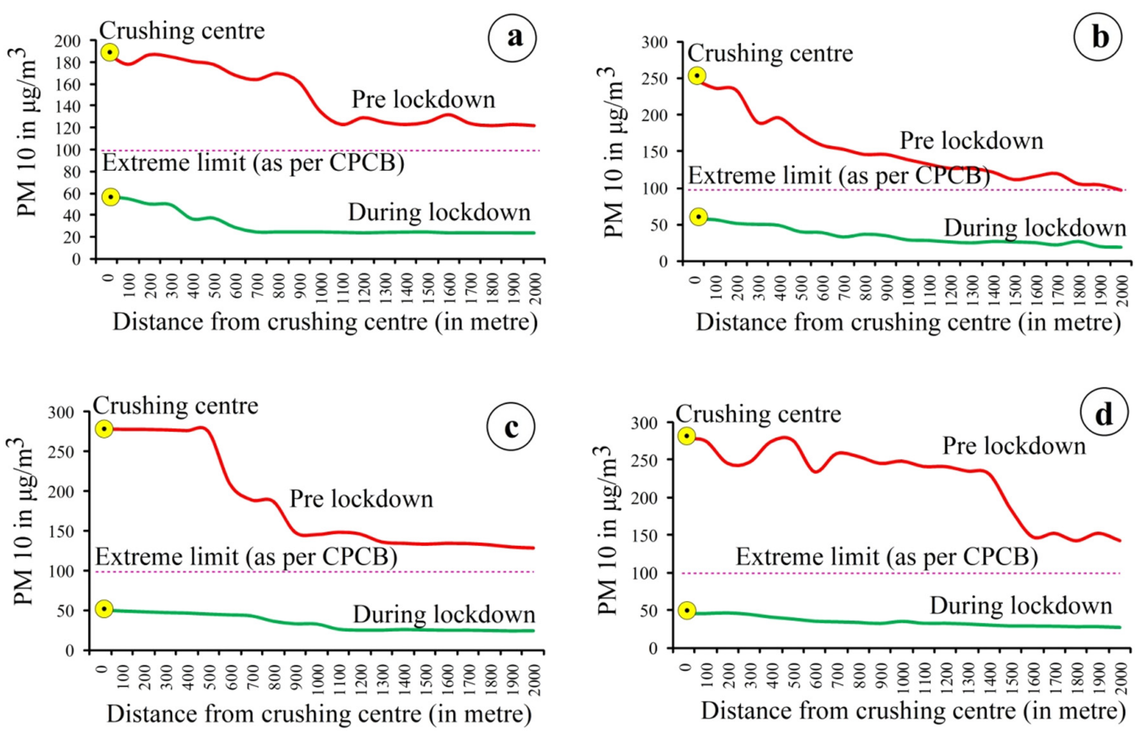

Fig. 3. Distance decay rate of PM_{10} concentration from crushing unit (12.03.2020 and 28.03.2020), average of 20 cross sections of PM_{10} in each clusters are taken into account for showing distance decay of particulate matter concentration (a) indicates PM_{10} change at cluster 1 (b) at cluster 2 (c) at cluster 3 and (d) at cluster 4.

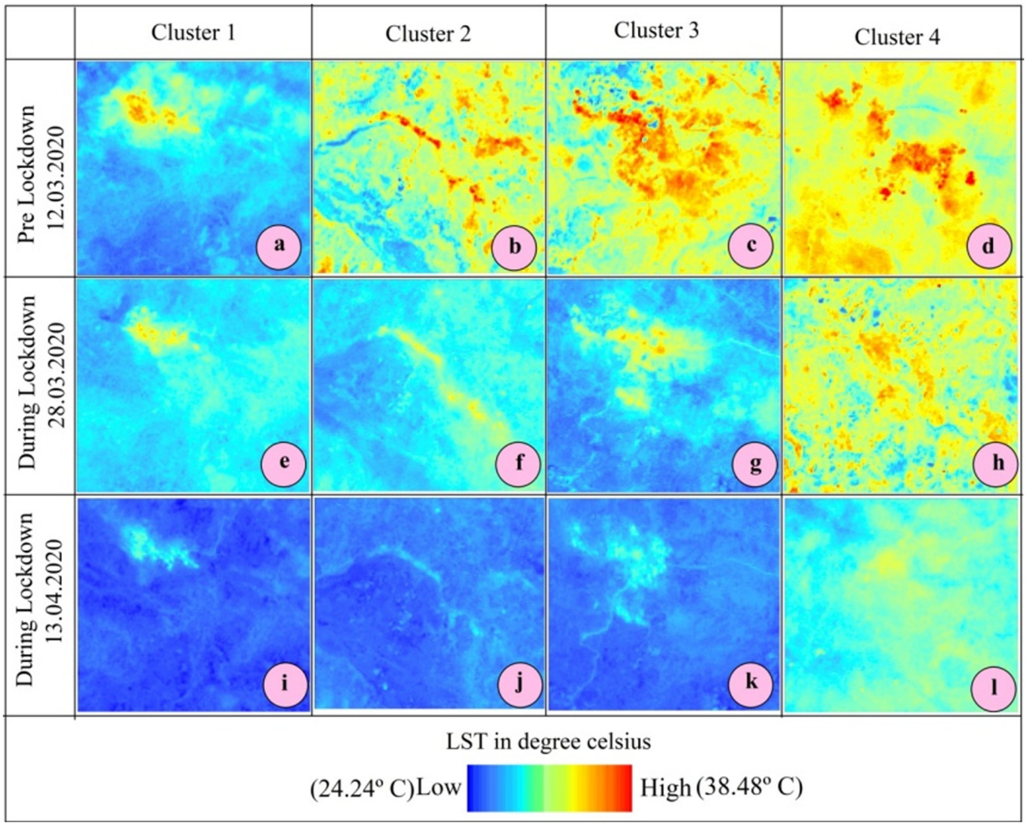

Fig. 4. Cluster specific LST in different phases.

units. According to the Central Pollution Control Board (CPCB), PM_{10} value over 100 is very dangerous to people, animals and the environment. In pre lockdown situation, the computed PM_{10} was 100 in all the clusters but it is considerably reduced amid lockdown situation mainly due to non-operational state of the quarrying and crushing units. For further specification, in clusters 1, 2, 3 and 4 the maximum levels of PM_{10} were 189.45, 248.49, 278.79 and 227.58, respectively. But the PM_{10} level is dropped to 59.67, 53.68, 49.58 and 64.88 μg/m^3 on those clusters as on 28th March 2020 (just after 4 days of commencing lockdown) (Table 2). The situation is further improved on 13.04.2020 (after 18 days of commencing lockdown). The degree of change is found high in the densely located crushing units. If areal coverage under different PM_{10} level of the study area is analyzed, it gives a satisfactory scenario showing declining areal extent under high PM level amid lockdown state (Table 3). In all the clusters about 50% area was characterized with PM_{10} level above 100 but amid lockdown entire area has registered PM level < 100.

To see the change of PM_{10} concentration from crushing unit to residential areas in pre lockdown period where crushers were in operational, the steep change is identified at the peripheral edge of the crushing unit but no such change is found between crushing unit and residential area (Fig. 3). The distance of steep change is different across the clusters and it is mainly due to areal extent of crusher concentration. This distance of steep change of PM_{10} is different at different directions from same crusher unit.

4.2. Effects on land surface temperature

Fig. 4 demonstrates spatial pattern of LST across the clusters in pre and during lockdown periods. Highest temperature is usually found in an around the stone quarrying and crushing units. A Pre lockdown LST record shows the fact. Historical time series LST on those areas also recorded high temperature in these areas and over the time with increasing density of crushing units the LST is registered high (Pal and Mandal, 2019a). This thermal condition adversely affects even the health of the workers and proximate local people. But amid lockdown the LST is reduced considerably. For instance, in pre lockdown period, maximum recorded temperature varies from 35.49 to 38.48 °C and just after 4 days of commencing lockdown it is reduced by 3.24–5.07 °C and 4 to 6.5 °C after 18 days. Average temperature of all the clusters ranged from 31.25 to 35.11 °C in pre lockdown period and it is reduced to 2.27 to 5.53 °C after 4 days and 2.74 to 7.06 °C after 18 days of commencing lockdown (Table 4). So the temperature recorded during operation of quarrying and crushing activities is not the sole effect of solar radiation. The reduced amount is due to the effect of anthropogenic activities.

Table 4
Clusterwise levels of LST value in Pre lockdown and during the lockdown periods (Values in °C).

Phase	Cluster 1			Cluster 2			Cluster 3			Cluster 4		
	Max.	Avg.	Min	Max.	Avg.	Min	Max.	Avg.	Min	Max.	Avg.	Min
12.03.2020	35.49	31.25	28.12	38.17	33.41	28.78	37.15	34.64	27.48	38.48	35.11	31.21
28.03.2020	30.58	28.54	26.43	33.10	28.49	27.47	32.11	29.11	25.12	35.24	32.37	28.55
13.04.2020	27.18	25.14	24.25	26.24	25.44	24.24	28.27	27.58	24.33	34.45	30.24	28.47

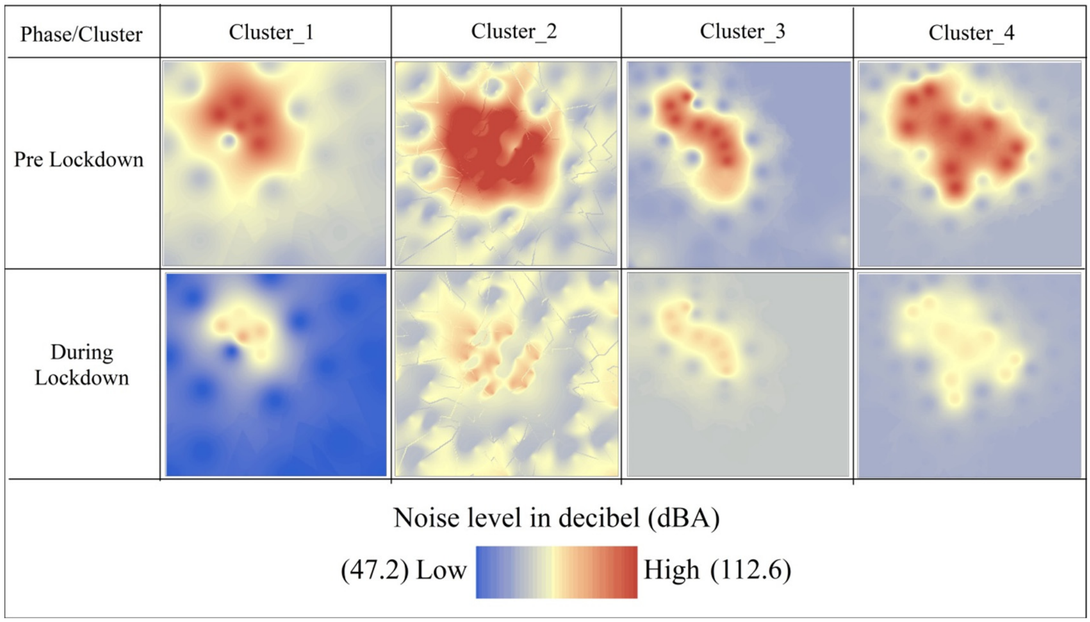

Fig. 5. Cluster wise ambiance noise level in pre lockdown and during the lockdown period.

4.3. Effects on noise ambience

During operational stage of crushers, noise pollution is very common. Noise level exceeds often 90dBA. In all the clusters from 8 am to 4 pm 35% to 68% falls under the noise level > 85dBA which is highly hazardous for human health (WHO, 2011). But incident of lockdown has turned this noise level quite normal like residential area or even less. In lockdown phase entire study units fall under the noise level < 65dBA which is normal as defined by CPCB (2009) (Fig. 5).

4.4. Effects on water quality of the river water

Huge amount of stone dust through air movement, drainage water discharge to river water and it causes change in water quality parameters. Pal and Mandal (2019a) reported adverse water quality beyond permissible limits in pre lockdown period. During lockdown water quality is significantly improved. TDS is maximally reduced in cluster 1 (2457 to 987) and in case of other clusters it is almost become half. DO level is also improved and all these are now within permissible limits (Table 5).

5. Discussion and conclusion

Result clearly exhibits that LST, PM_{10} concentration, noise level and river water quality have reduced significantly and all these are under CPCB, WHO defined ambient quality level after commencing lockdown. In pre lockdown state when all the industrial units are in operational state, the effect is recorded hazardous to environment components in general and human health in particular (Pal and Mandal, 2019a, 2019b; Venter et al., 2020; Muhammad et al., 2020). Continuous emission of dust particles crushed due to stone crushing since morning to evening add huge volume of dust into the atmosphere, water body and contaminate the quality of air and water. Particulate matter concentration above 100 is harmful for human health (WHO, 2006). Inhaling fine dust particles for long time often creates different respiratory diseases and also invite deaths (WHO, 2006; WHO, 2016; WHO, 2018). Around 29% of lung cancer deaths, 24% stroke deaths, 25% cardiac disease death and 43% other lung disease are reported to be causing air pollution (Wu et al., 2020). Also, air pollution caused 26% deaths from respiratory illness, 25% deaths from COPD and some 17% deaths from ischemic heart and stroke (WHO, 2020). At this point, it should be noted that for those with chronic respiratory and cardiovascular disorders, the COVID-19 death rate is significantly higher. Such diseases are also related to air pollution, which means air pollution can be seen as a secondary factor in these deaths (Wang et al., 2020; Travaglio et al., 2020). Past studies have verified the effect of air pollution on the health conditions. Several studies have shown that air pollution exposure has that health risks linked with respiratory, cardiovascular, pulmonary and other results related to health in the past decades, creating significant interest in air pollution (Karimzadegan et al., 2008; Xing et al., 2016; Isaifan, 2020; Peshave and Peshave, 2020). In their previous studies, Pal and Mandal (2019a, b) showed how the stone quarrying and crushing process is adding dust particles to the air day after day. They have estimated aerosol concentration from the region from 2014 to 2017 in seasonwise at lower atmosphere. The average PM_{10} value in summer season was 183.24 and winter PM_{10} value was 224.33. So it is important to say that the PM_{10} value is always very high in this area. But temporary closure of quarrying and crushing units has reduced this level significantly and it is good for human health. The people is already affected by PM related diseases may get temporary relief. Due to continuous release of heat from the crusher machine, temperature also found high in

Table 5
Clusterwise water quality parameters in pre and during lockdown periods.

Water quality parameters	Cluster 1		Cluster 2		Cluster 3		Cluster 4	
	a	b	a	b	a	b	a	b
pH	8.7	6.9	8.9	7.1	8.7	7.3	8.8	7.6
DO (ppm.)	3.74	4.12	3.18	4.32	3.14	4.43	2.72	3.25
TDS (mg/l.)	2457	987	2369	1124	2415	1023	2289	1289

a: pre lockdown phase; b: after 30 days of commencing lockdown.

the industrial area (Pal and Mandal, 2017; Pal and Mandal, 2019a; Pal and Mandal, 2019b; Geissbühler et al., 2016). This result although is associated with a regional scale study but a few study already done by Saadat et al. (2020), Sharma et al. (2020), Wang and Su (2020), Wang et al. (2020), Tobías et al. (2020), Bashir et al. (2020) have also reported the diminishing PM level concentration in air along with other greenhouse gases.

Lockdown condition has recorded about 3–5 °C temperature less than pre lockdown period indicating the fact that industry induced energy footprint enhances temperature significantly. Due to non-operational state the noise level is ambient and found suitable for human health. River water quality is improved significantly amid lockdown. Usually huge amount of dust admixing with drainage debouches to nearby river and change the normal water quality parameters like total dissolved solid, temperature, pH, turbidity, dissolved oxygen etc. (Pal and Mandal, 2019b). As no such admixing is taking place amid lockdown, since water quality is improved. CPCB (2020a,b) reported same incidents of water quality improvement in river Ganga, Yamuna amid lockdown situation.

However this incident clearly pointed out a way through which we can combat pollution of different environmental components and human health. Temporary lockdown can improve the quality of environment. It may hamper the economy but if we think about sustainable economy, sustainable economy in co-existence with ambient environment it is the only way. Worldwide lock down has provided a good opportunity to realize our pressure on nature and patience of nature. However successful control of pollution sources can give a lively earth and it can establish the right to life in our planet earth.

CRediT authorship contribution statement

Indrajit Mandal: Resources.**Swades Pal:**Conceptualization, Writing - review & editing, Writing - original draft.

Declaration of competing interest

None.

The authors whose names are listed certify that they have NO affiliations with or involvement in any organization or entity with any financial interest (such as honoraria; educational grants; participation in speakers' bureaus; membership, employment, consultancies, stock ownership, or other equity interest; and expert testimony or patent-licensing arrangements), or non-financial interest (such as personal or professional relationships, affiliations, knowledge or beliefs) in the subject matter or materials discussed in this manuscript. With regards.

References

Abdullah, S., Mansor, A.A., Napi, N.N.L.M., Mansor, W.N.W., Ahmed, A.N., Ismail, M., Ramly, Z.T.A., 2020. Air quality status during 2020 Malaysia Movement Control Order (MCO) due to 2019 novel coronavirus (2019-nCoV) pandemic. Sci. Total Environ. 729, 139022. https://doi.org/10.1016/j.scitotenv.2020.139022.

Alvarez-Mendoza, C.I., Teodoro, A.C., Torres, N., Vivanco, V., 2019. Assessment of remote sensing data to model PM10 estimation in cities with a low number of air quality stations: a case of study in Quito, Ecuador. Environments 6, 1–15. https://doi.org/10.3390/environments6070085.

Andersson, D., Nässén, J., 2016. Should environmentalists be concerned about materialism? An analysis of attitudes, behaviours and greenhouse gas emissions. J. Environ. Psychol. 48, 1–11.

Anjum, N.A., 2020. Good in the Worst: COVID-19 Restrictions and Ease in Global Air Pollution. https://doi.org/10.20944/preprints202004.0069.v1.

Artis, D.A., Carnahan, W.H., 1982. Survey of emissivity variability in thermography of urban areas. Remote Sens. Environ. 12, 313–329.

Bashir, M.F., Ma, B., Komal, B., Bashir, M.A., Tan, D., Bashir, M., 2020. Correlation between climate indicators and COVID-19 pandemic in New York, USA. Sci. Total Environ. 728 (2020), 01–03. https://doi.org/10.1016/j.scitotenv.2020.138835 138835.

Becchetti, L., Conzo, G., Conzo, P., Salustri, F., 2020. Understanding the Heterogeneity of Adverse COVID-19 Outcomes: The Role of Poor Quality of Air and Lockdown Decisions (Available at SSRN 3572548).

Beine, M., Bertoli, S., Chen, S., D'Ambrosio, C., Docquier, F., Dupuy, A., Fusco, A., Girardi, S., Haas, T., Islam, N., Koulovatianos, C., 2020. Economic Effects of Covid-19 in Luxembourg.

Cadotte, M., 2020. Early Evidence that COVID-19 Government Policies Reduce Urban Air Pollution. https://doi.org/10.31223/osf.io/nhgj3.

Chander, G., Markham, B.L., Helder, D.L., 2009. Summary of current radiometric calibration coefficients for Landsat MSS, TM, ETM+, and EO-1 ALI sensors. Remote Sens. Environ. 113, 893–903. https://doi.org/10.1016/j.rse.2009.01.007.

Chitranshi, S., Sharma, S.P., Dey, S., 2015. Spatio-temporal variations in the estimation of PM10from MODIS-derived aerosol optical depth for the urban areas in the Central Indo-Gangetic Plain. Meteorog. Atmos. Phys. 127, 107–121. https://doi.org/10.1007/s00703-014-0347-z.

Chowdhury, S., Dey, S., Di Girolamo, L., Smith, K.R., Pillarisetti, A., Lyapustin, A., 2019. Tracking ambient PM2.5 build-up in Delhi national capital region during the dry season over 15 years using a high-resolution (1 km) satellite aerosol dataset. Atmos. Environ. 204, 142–150. https://doi.org/10.1016/j.atmosenv.2019.02.029.

CPCB, 2009. Comprehensive industry document stone crushers, central pollution control board, Govt. of India. Series: COINDS/78/2007-08, 1.1 – 8.21.

CPCB, 2020. Impact of lockdown (25th March to 15th April) on air quality. Ministry of Environment, Forest and Climate Change) Govt. of India, Delhi, pp. 1–62. https://cpcb.nic.in/latest-cpcb.php.

Das, S., Ghosh, P., Sen, B., Mukhopadhyay, I., 2020. Critical Community Size for COVID-19– a Model Based Approach to Provide a Rationale behind the Lockdown (arXiv preprint arXiv:2004.03126).

Dutheil, F., Baker, J.S., Navel, V., 2020. COVID-19 as a factor influencing air pollution? Environmental Pollution (Barking, Essex: 1987) https://doi.org/10.1016/j.envpol.2020.114466.

European Space Agency, 2020. COVID-19: nitrogen dioxide over China. https://www.esa.int/Applications/Observing_the_Earth/Copernicus/Sentinel-5P/COVID19_nitrogen_dioxide_over_China.

Geissbühler, L., Kolman, M., Zanganeh, G., Haselbacher, A., Steinfeld, A., 2016. Analysis of industrial-scale high-temperature combined sensible/latent thermal energy storage. Appl. Therm. Eng. 101, 657–668.

Han, Y., Lam, J.C., Li, V.O., Guo, P., Zhang, Q., Wang, A., Crowcroft, J., Wang, S., Fu, J., Gilani, Z., Downey, J., 2020. The Effects of Outdoor Air Pollution Concentrations and Lockdowns on Covid-19 Infections in Wuhan and Other Provincial Capitals in China. https://doi.org/10.20944/preprints202003.0364.v1.

He, G., Pan, Y., Tanaka, T., 2020. COVID-19, City Lockdowns, and Air Pollution: Evidence from China. *medRxiv*. https://doi.org/10.1101/2020.03.29.20046649.

Huang, X., Ding, A., Gao, J., Zheng, B., Zhou, D., Qi, X., Tang, R., Ren, C., Nie, W., Chi, X., Wang, J., 2020. Enhanced Secondary Pollution Offset Reduction of Primary Emissions during COVID-19 Lockdown in China. https://doi.org/10.31223/osf.io/hvuzy.

Isaifan, R.J., 2020. The dramatic impact of Coronavirus outbreak on air quality: has it saved as much as it has killed so far? Global Journal of Environmental Science and Management 6 (3), 275–288. https://doi.org/10.22034/GJESM.2020.03.01.

Jerez, S., López-Romero, J.M., Turco, M., Jiménez-Guerrero, P., Vautard, R., Montávez, J.P., 2018. Impact of evolving greenhouse gas forcing on the warming signal in regional climate model experiments. Nat. Commun. 9 (1), 1–7.

Kambalagere, Y., 2020. A study on Air Quality Index (AQI) of Bengaluru, Karnataka during lockdown period to combat coronavirus disease (Covid-19): air quality turns 'Better' from 'Hazardous'. Studies in Indian Place Names 40 (69), 59–66.

Karimzadegan, H., Rahmatian, M., Farhud, D.D., Yunesian, M., 2008. Economic valuation of air pollution health impacts in the Tehran Area, Iran. Iran. J. Public Health, 20–30. http://ijph.tums.ac.ir/index.php/IJPH/article/view/2068.

Kelly, F.J., Fussell, J.C., 2015. Air pollution and public health: emerging hazards and improved understanding of risk. Environ. Geochem. Health 37 (4), 631–649.

Koelemeijer, R.B.A., Homan, C.D., Matthijsen, J., 2006. Comparison of spatial and temporal variations of aerosol optical thickness and particulate matter over Europe. Atmos. Environ. 40, 5304–5315. https://doi.org/10.1016/j.atmosenv.2006.04.044.

Landsat Project Science Office, 2002. Landsat 7 Science Data User's Handbook. Goddard Space FlightCenter, NASA, Washington, DC http://ltpwww.gsfc.nasa.gov/IAS/handbook/handbook_toc.html.

Lau, H., Khosrawipour, V., Kocbach, P., Mikolajczyk, A., Schubert, J., Bania, J., Khosrawipour, T., 2020. The positive impact of lockdown in Wuhan on containing the COVID-19 outbreak in China. Journal of Travel Medicine 37 (2020), 01–14. https://doi.org/10.1093/jtm/taaa037.

Lauri, M., 2020. Analysis: Corona virus has temporarily reduced Chins's CO2 emissions by534 a quarter. CarbonBrief (Retrieved 01 April 2020). https://www.carbonbrief.org/analysis-coronavirus-has-temporarily-reduced-chinas-co2-emissions-by-a-quarter.

Layard, R., Clark, A., De Neve, J.E., Krekel, C., Fancourt, D., Hey, N., O'Donnell, G., 2020. When to Release the Lockdown? A Wellbeing Framework for Analysing Costs and Benefits.

Lee, H.J., Liu, Y., Coull, B.A., Schwartz, J., Koutrakis, P., 2011. A novel calibration approach of MODIS AOD data to predict $PM_{2.5}$ concentrations. Atmos. Chem. Phys. 11, 7991–8002. https://doi.org/10.5194/acp-11-7991-2011.

Ma, Y., Zhao, Y., Liu, J., He, X., Wang, B., Fu, S., Yan, J., Niu, J., Zhou, J., Luo, B., 2020. Effects of temperature variation and humidity on the death of COVID-19 in Wuhan, China. Sci. Total Environ., 138226 https://doi.org/10.1016/j.scitotenv.2020.138226 (March, 2020).

Mahato, S., Pal, S., Ghosh, K.G., 2020. Effect of lockdown amid COVID-19 pandemic on air quality of the megacity Delhi, India. Sci. Total Environ. 730. https://doi.org/10.1016/j.scitotenv.2020.139086.

Manabe, S., 2019. Role of greenhouse gas in climate change. Tellus A: Dynamic Meteorology and Oceanography 71 (1), 1–13.

Mate, A., Killian, J.A., Wilder, B., Charpignon, M., Awasthi, A., Tambe, M., Majumder, M.S., 2020. Evaluating COVID-19 Lockdown Policies for India: A Preliminary Modeling Assessment for Individual States. Available at SSRN 3575207. https://doi.org/10.2139/ssrn.3575207.

Mathur, B.H., Sudheer, G.K., Sanchana, M., Boddu, C., Aravinth, J., 2020, March. High resolution air pollution mapping using wireless sensor nodes. 2020 6th International

Conference on Advanced Computing and Communication Systems (ICACCS). IEEE, pp. 430–435. https://doi.org/10.1109/ICACCS48705.2020.9074396.
McMahon, J., 2020. Study: coronavirus lockdown likely saved 77,000 lives in China just by reducing pollution, Forbes. https://www.forbes.com/sites/jefmcmahon/2020/03/16/coronaviruslockdownmay-have-saved-77000-lives-in-china-just-from-pollution-reduction/#2e94bd3f34fe, Accessed date: 19 March 2020.
Mitra, A., Chaudhuri, T.R., Mitra, A., Pramanick, P., Zaman, S., Mitra, A., Chaudhuri, T.R., Mitra, A., Pramanick, P., Zaman, S., 2020. Impact of COVID-19 related shutdown on atmospheric carbon dioxide level in the city of Kolkata. Science and Education 6 (3), 84–92.
Muhammad, S., Long, X., Salman, M., 2020. COVID-19 pandemic and environmental pollution: a blessing in disguise? Sci. Total Environ., 138820 https://doi.org/10.1016/j.scitotenv.2020.138820.
Nadzri, O., Mohd, Z.M.J., Lim, H.S., 2010. Estimating particulate matter concentration over arid region using satellite remote sensing: a case study in Makkah, Saudi Arabia. Mod. Appl. Sci. 4, 131–142.
Ogen, Y., 2020. Assessing nitrogen dioxide (NO2) levels as a contributing factor to coronavirus (COVID-19) fatality. Sci. Total Environ. 726, 138605. https://doi.org/10.1016/j.scitotenv.2020.138605.
Olmanson, L.G., Brezonik, P.L., Finlay, J.C., Bauer, M.E., 2016. Comparison of Landsat 8 and Landsat 7 for regional measurements of CDOM and water clarity in lakes. Remote Sensing of Environment 185, 119–128. https://doi.org/10.1016/j.rse.2016.01.007.
Pal, S., Mandal, I., 2017. Impacts of stone mining and crushing on stream characters and vegetation health of Dwarka river basin of Jharkhand and West Bengal, Eastern India. Journal of Environmental Geography 10 (1–2), 11–21. https://doi.org/10.1515/jengeo-2017-0002.
Pal, S., Mandal, I., 2019a. Impacts of stone mining and crushing on environmental health in Dwarka river basin. Geocarto International, 1–29 https://doi.org/10.1080/10106049.2019.1597390.
Pal, S., Mandal, I., 2019b. Impact of aggregate quarrying and crushing on socio-ecological components of Chottanagpur plateau fringe area of India. Environ. Earth Sci. 78, 661. https://doi.org/10.1007/s12665-019-8678-1.
Peshave, J., Peshave, M., 2020. Covid-19 lockdown–a blessing or curse. CLIO An Annual Interdisciplinary Journal of History 6 (1), 537–544.
Raffaelli, K., Deserti, M., Stortini, M., Amorati, R., Vasconi, M., Giovannini, G., 2020. Improving air quality in the Po Valley, Italy: some results by the LIFE-IP-PREPAIR project. Atmosphere 11 (4), 429. https://doi.org/10.3390/atmos11040429.
Ray, D., Salvatore, M., Bhattacharyya, R., Wang, L., Mohammed, S., Purkayastha, S., Halder, A., Rix, A., Barker, D., Kleinsasser, M., Zhou, Y., 2020. Predictions, Role of Interventions and Effects of a Historic National Lockdown in India's Response to the COVID-19 Pandemic: Data Science Call to Arms. medRxiv. https://doi.org/10.1101/2020.04.15.20067256.
Saadat, S., Rawtani, D., Hussain, C.M., 2020. Environmental perspective of COVID-19. Sci. Total Environ., 138870 https://doi.org/10.1016/j.scitotenv.2020.138870.
Sharma, S., Zhang, M., Gao, J., Zhang, H., Kota, S.H., 2020. Effect of restricted emissions during COVID-19 on air quality in India. Sci. Total Environ. 728, 138878. https://doi.org/10.1016/j.scitotenv.2020.138878.
Snyder, W.C., Wan, Z., Zhang, Y., Feng, Y.Z., 1998. Classification-based emissivity for Land Surface Temperature measurement from space. Int. J. Remote Sens. 19 (14), 2753–2774.
Sobrino, J.A., Jiménez-Muñoz, J.C., Paolini, L., 2004. Land surface temperature retrieval from LANDSAT TM 5. Remote Sens. Environ. 90, 434–440. https://doi.org/10.1016/j.rse.2004.02.003.
Sohrabi, C., Alsafi, Z., O'Neill, N., Khan, M., Kerwan, A., Al-Jabir, A., Iosifidis, C., Agha, R., 2020. World Health Organization declares global emergency: a review of the 2019 novel coronavirus (COVID-19). Int. J. Surg. https://doi.org/10.1016/j.ijsu.2020.02.034.
Tobías, A., Carnerero, C., Reche, C., Massagué, J., Via, M., Minguillón, M.C., Alastuey, A., Querol, X., 2020. Changes in air quality during the lockdown in Barcelona (Spain) one month into the SARS-CoV-2 epidemic. Sci. Total Environ., 138540 https://doi.org/10.1016/j.scitotenv.2020.138540.
Tonne, C., Halonen, J.I., Beevers, S.D., Dajnak, D., Gulliver, J., Kelly, F.J., ... Anderson, H.R., 2016. Long-term traffic air and noise pollution in relation to mortality and hospital readmission among myocardial infarction survivors. International journal of hygiene and environmental health 219 (1), 72–78.
Travaglio, M., Popovic, R., Yu, Y., Leal, N., Martins, L.M., 2020. Links between Air Pollution and COVID-19 in England.medRxiv. https://doi.org/10.1101/2020.04.16.20067405.
Venter, Z.S., Aunan, K., Chowdhury, S., Lelieveld, J., 2020. COVID-19 Lockdowns Cause Global Air Pollution Declines with Implications for Public Health Risk (medRxiv).
Wang, P., Chen, K., Zhu, S., Wang, P., Zhang, H., 2020. Severe air pollution events not avoided by reduced anthropogenic activities during COVID-19 outbreak. Resour. Conserv. Recycl. 158, 104814.
Wang, Q., Su, M., 2020. A preliminary assessment of the impact of COVID-19 on environment–a case study of China. Sci. Total Environ., 138915 https://doi.org/10.1016/j.scitotenv.2020.138915.
Watts, J., Kommenda, N., 2020. Coronavirus pandemic leading to huge drop in airpollution. The Guardian (Retrieved 4 April 2020). https://www.theguardian.com/environment/2020/mar/23/coronavirus-pandemic-leading-to-huge-drop-in-air-pollution.
WHO, 2011. Burden of disease from environmental noise: Quantification of healthy life years lost in Europe. Burden of Disease from Environmental Noise: Quantification of Healthy Life Years Lost in Europe. WHO, Regional Office for Europe, pp. 1–106.
WHO, 2012. Global estimates on prevalence of hearing loss mortality and burden of diseases and prevention of blindness and deafness. www.who.int/pbd/deafness/WHO_GE_HL.pdf.
WHO, 2020. Coronavirus Disease 2019 (COVID-19): Situation Report. p. 36.
World Health Organization, 2006. WHO Air Quality Guidelines for Particulate Matter, Ozone, Nitrogen Dioxide and Sulfur Dioxide: Global Update 2005: Summary of Risk Assessment (No. WHO/SDE/PHE/OEH/06.02). World Health Organization, Geneva.
World Health Organization, 2016. Ambient Air Pollution: A Global Assessment of Exposure and Burden of Disease. World Health Organization (ISBN: 9789241511353).
World Health Organization,2018. Ambient outdoor air quality and health. Downloaded from www.who.int/news-room/factsheets/detail/ambient-(outdoor)-air-quality-and-health, on 30.
Wu, X., Nethery, R.C., Sabath, B.M., Braun, D., Dominici, F., 2020. Exposure to Air Pollution and COVID-19 Mortality in the United States. *medRxiv*. https://doi.org/10.1101/2020.04.05.20054502.
Wu, Y., Zhang, S., Hao, J., Liu, H., Wu, X., Hu, J., Walsh, M.P., Wallington, T.J., Zhang, K.M., Stevanovic, S., 2017. On-road vehicle emissions and their control in China: a review and outlook. Sci. Total Environ. 574, 332–349. https://doi.org/10.1016/j.scitotenv.2016.09.040.
Xing, Y.F., Xu, Y.H., Shi, M.H., Lian, Y.X., 2016. The impact of PM2.5 on the human respiratory system. Journal of Thoracic Disease 8 (1), E69. https://doi.org/10.3978/j.issn.2072-1439.2016.01.19.
Yap, X.Q., Hashim, M., 2013. A robust calibration approach for PM10 prediction from MODIS aerosol optical depth. Atmos. Chem. Phys. 13, 3517–3526. https://doi.org/10.5194/acp-13-3517-2013.
Yap, X.Q., Hashim, M., Marghany, M., 2011. Retrieval of PM_{10} concentration from Moderate Resolution Imaging Spectroradiometer (MODIS) derived AOD in peninsular Malaysia. Geoscience and Remote Sensing Symposium (IGARSS). IEEE International, pp. 4022–4025.
Yongjian, Z., Jingu, X., Fengming, H., Liqing, C., 2020. Association between short-term exposure to air pollution and COVID-19 infection: evidence from China. Sci. Total Environ., 138704 https://doi.org/10.1016/j.scitotenv.2020.138704.
Zhang, X., Wang, H., Che, H.Z., Tan, S.C., Shi, G.Y., Yao, X.P., 2020. The impact of aerosol on MODIS cloud detection and property retrieval in seriously polluted East China. Sci. Total Environ. 711, 134634. https://doi.org/10.1016/j.scitotenv.2019.134634.